Acta Materialia 239 (2022) 118279

Contents lists available at ScienceDirect

Acta Materialia

journal homepage: www.elsevier.com/locate/actamat

Hydrogen-enhanced grain boundary vacancy stockpiling causes transgranular to intergranular fracture transition

Yu Ding[a], Haiyang Yu[b,*], Meichao Lin[a], Kai Zhao[c], Senbo Xiao[a], Alexey Vinogradov[d], Lijie Qiao[e], Michael Ortiz[f], Jianying He[a,*], Zhiliang Zhang[a,*]

[a] Department of Structural Engineering, Norwegian University of Science and Technology (NTNU), Trondheim 7491, Norway
[b] Division of Applied Mechanics, Department of Materials Science and Engineering, Uppsala University, Uppsala 75121, Sweden
[c] Jiangsu Key Laboratory of Advanced Food Manufacturing Equipment and Technology, Jiangnan University, Wuxi 214122, China
[d] Department of Mechanical and Industrial Engineering, Norwegian University of Science and Technology (NTNU), Trondheim 7491, Norway
[e] Beijing Advanced Innovation Center for Materials Genome Engineering, University of Science and Technology Beijing, Beijing 100083, China
[f] Graduate Aerospace Laboratories, California Institute of Technology, 1200 E. California Blvd., Pasadena, CA 91125, USA

ARTICLE INFO

Article history:
Received 24 April 2022
Revised 8 August 2022
Accepted 15 August 2022
Available online 17 August 2022

Keywords:
Hydrogen embrittlement
Intergranular failure
Vacancies
Grain boundaries
Molecular dynamics (MD)

ABSTRACT

The attention to hydrogen embrittlement (HE) has been intensified recently in the light of hydrogen as a carbon-free energy carrier. Despite worldwide research, the multifaceted HE mechanism remains a matter of debate. Here we report an atomistic study of the coupled effect of hydrogen and deformation temperature on the pathway to intergranular fracture of nickel. Uniaxial straining is applied to nickel $\Sigma5(210)[001]$ and $\Sigma9(1\text{-}10)[22\text{-}1]$ grain boundaries with or without pre-charged hydrogen at various temperatures. Without hydrogen, vacancy generation at grain boundary is limited and transgranular fracture mode dominates. When charged, hydrogen as a booster can enhance strain-induced vacancy generation by up to ten times. This leads to the superabundant vacancy stockpiling at the grain boundary, which agglomerates and nucleates intergranular nanovoids eventually causing intergranular fracture. While hydrogen tends to persistently enhance vacancy concentration, temperature plays an intriguing dual role as either an enhancer or an inhibitor for vacancy stockpiling. These results show good agreement with recent positron annihilation spectroscopy experiments. An *S*-shaped quantitative correlation between the proportion of intergranular fracture and vacancy concentration was for the first time derived, highlighting the existence of a critical vacancy concentration, beyond which fracture mode will be completely intergranular.

1. Introduction

The phenomenon of hydrogen in metals causing catastrophic degradation of mechanical properties, including strength, ductility, and fracture toughness, is known as hydrogen embrittlement (HE). Substantial efforts have been devoted to deciphering the genesis of this phenomenon at different scales since it was first observed in 1875 [1,2]. However, the fundamental mechanism of HE remains a matter of debate because of its multifaceted nature. The primary controversy is over the role of plasticity in hydrogen-induced degradation. Many theories have been proposed in this respect [3–6], and to name only a few, hydrogen-enhanced decohesion (HEDE) and hydrogen-enhanced localized plasticity (HELP). The HEDE mechanism postulates that dissolved hydrogen at a grain boundary (GB) or crack tip weakens interatomic bonds, thus reducing the fracture energy [7]. It reflects the nature of embrittlement and has been widely employed to rationalize the hydrogen-induced ductile to brittle transition [8–11]. However, HEDE does not explicitly address the intensive plasticity seemingly promoted by hydrogen, as revealed in many experiments [12,13]. In contrast, the HELP [14] mechanism regards hydrogen as an enhancer for dislocation mobility, as evidenced by a number of transmission electron microscopy (TEM) observations [15]. However, recent atomistic modeling [16] and *in-situ* experimental observation [17] showed that dislocation motion could be hindered by the Cottrell atmosphere built up by hydrogen. These contradictory results reflect the complexity of the interactions between plasticity and hydrogen when examined at different spatial and temporal scales.

Dislocation is not the sole carrier of plasticity, other types of defects such as GB and vacancy also exert an influence through

* Corresponding authors.
E-mail addresses: haiyang.yu@angstrom.uu.se (H. Yu), jianying.he@ntnu.no (J. He), zhiliang.zhang@ntnu.no (Z. Zhang).

https://doi.org/10.1016/j.actamat.2022.118279

their interaction with hydrogen. In polycrystalline materials, the embrittlement is usually accompanied by a transition from transgranular to intergranular fracture [18,19]. This transition has been attributed to decohesion caused by hydrogen segregation at GBs [20,21]. By observing extensive dislocation substructures beneath the intergranular fracture surface, Robertson et al. [5,22] claimed that hydrogen-enhanced dislocation activity was the necessary precursor for intergranular fracture. It should be noted that this conclusion is a posteriori interpretation of microstructural features observed after failure, whereas a time-resolved nanoscale mechanism is still lacking.

Superabundant vacancies have been shown to form in many hydrogen-metal systems [23]. With aid of positron annihilation spectroscopy (PAS), Nagumo et al. [24,25] pointed out the predominant role of vacancies in premature fracture, which is referred to as hydrogen-enhanced strain-induced vacancies (HESIV) mechanism. Hydrogen stabilizes vacancies by forming hydrogen-vacancy complex (Va-H) and participates in subsequent plastic deformation [17,26,27]. However, the direct connection between superabundant vacancies and the final intergranular fracture remains a mystery. Recent PAS experiments by Lawrence et al. [28] showed that the hydrogen-enhanced vacancy generation becomes more pronounced in fine-grained nickel alloys as temperature decreases, and the propensity for intergranular failure is also amplified [29,30]. These observations call for an in-depth investigation of the nanoscale interactions among hydrogen, vacancy, and GB.

It is still very challenging today to track hydrogen atoms precisely by experiment [31,32]. As a result, knowledge about hydrogen-microstructure interactions is limited. Atomistic modeling has proven as a powerful alternative tool for probing the nanoscale mechanisms of HE [9,10,15,17,33–35]. The atomistic studies of HE have been divided into several sub-processes, i.e., vacancy formation [36–38], dislocation dynamics [39–41], intergranular decohesion [42–44], and crack propagation [45–47]. In these studies, the respective contributions of hydrogen-influenced dislocation and vacancy to the intergranular fracture transition have been treated ambiguously. In order to explore a nanoscale mechanism that can directly link to the intergranular fracture transition, we employ atomistic modeling to study HE in bi-crystal nickel. Uniaxial straining tests with two representative GBs are carried out at varying hydrogen concentrations and temperatures, focusing on the time-resolved evolution of dislocations and vacancies as well as their contribution to the final separation of GBs. A large number of repeated simulations are performed for each condition to obtain a statistical representation of the results. The study enables quantification of the individual roles played by hydrogen, temperature, dislocations and vacancies in the transition to intergranular fracture. A quantitative relationship between vacancy concentration and intergranular fracture is for the first time derived to highlight the threshold vacancy concentration for fully intergranular fracture. The present findings unveil a nanoscale mechanism for intergranular fracture transition, more importantly, allow for the establishment of a quantitative mechanism-based prediction of HE.

2. Methodology

We utilized large-scale atomistic simulations to investigate the deformation behavior of the nickel-hydrogen system, focusing on the microstructure evolution during the hydrogen-induced intergranular fracture transition process. The atomic interactions were described by the embedded atom method potential developed by Angelo [48], which is widely adopted to study the deformation behavior of nickel [49–51]. The molecular dynamic (MD) simulations were performed using the LAMMPS code [52].

Two nickel bicrystal models were established with Σ5(210)[001] symmetric tilt GB and Σ9(1-10)[22-1] pure twist GB. Σ is the reciprocal density of coincident sites; (210) and (1-10) represent the GB planes, and [001] and [22-1] are the tilt or twist axes. The Σ5 and Σ9 GBs represent typical low-Σ and general GBs, respectively. The models were assumed to be in the vicinity of a crack tip, subjected to high stress triaxiality. An illustration was given in Fig. 1. The GBs were created by constructing two separate crystals with desired crystallographic orientations in a rectangular simulation box and then aligning the crystals along a plane normal to the Y-direction. Periodic boundary conditions were applied along the X and Z directions, while free boundary condition was employed along the Y direction. The initial configuration was then modified by shifting the upper grain in the X-Z plane, deleting overlapping atoms, and applying the conjugate gradient method to equilibrate the system. The resulting simulation box dimensions (L_x, L_y, L_z) were (11.9 nm, 23.8 nm, 10.6 nm) and (10.6 nm, 20.1 nm, 9.1 nm) for Σ5 and Σ9, respectively. All the simulation boxes were divided into three regions: the area 1 nm above and below the GB was referred to as the GB region, the 1 nm thick regions at the top and bottom of the simulation box were fixed as rigid blocks for the application of displacement, and the remaining was regarded as grain interior.

After relaxation in the isothermal–isobaric (NPT) ensemble at 300 K for 100 ps, the hybrid grand canonical Monte Carlo (GCMC)/molecular dynamic method [19] was utilized to obtain hydrogen distribution in the samples. The procedure consists of loops of hydrogen charging GCMC steps and subsequent MD steps and provides a hydrogen segregation map without considering the kinetic process, which would otherwise take a formidable long time in a pure MD simulation. At each GCMC step [53], hydrogen atoms were randomly inserted/deleted in the boxes in order to achieve a target chemical potential μ within a constant volume V and temperature T. In the end, the equilibrium hydrogen distribution in GB and grain interior will be under the same chemical potential μ. There exists a relationship between the chemical potential μ and the locally equilibrated hydrogen concentration c:

$$\mu = kTlnc + \triangle E, \tag{1}$$

where $\triangle E$ is the local segregation energy of one hydrogen atom and k is the Boltzmann constant. For all the cases, $\mu = -2.31$ eV was chosen as the charging potential which corresponds to the bulk hydrogen concentration in grains $c_0 = 0.001$ (H/Ni atomic ratio). This hydrogen concentration is in agreement with previous experiments [28,29]. In the subsequent MD steps, a canonical (NVT) ensemble was applied to equilibrate the system at $T = 300$ K after every hydrogen charging step. Each GCMC step was followed by 50 MD steps until the hydrogen concentration in the box fluctuated in a narrow range (±1% atomic ratio). The equilibrium hydrogenated GB after charging was regarded as a 100% saturation case, and the 0%, 13%, 25%, 40%, 60% saturation cases were simulated for comparison. All samples in these cases were further equilibrated at 77 K, 300 K, and 600 K in the NPT ensemble for 100 ps. Then uniaxial straining was applied in the NVT ensemble at the three temperatures by moving the upper boundary layer at a constant velocity along the Y direction while the lower layer was kept stationary. This loading method provides a high stress triaxiality and mimics the mechanical behavior close to the crack tip. In total, we had 2 GB types × 6 hydrogen concentrations × 3 temperatures = 36 different conditions. For each condition, we performed 20 independent mechanical tests with random temperature seeds. This guarantees statistical significance in capturing the thermal effect during mechanical deformation and produces the basis for calculating the intergranular fracture fraction.

The atomic stress during deformation was analyzed by Viral theory [54]. The local atomistic structures in the system were characterized by the centro-symmetry parameter (CSP) [55] and common neighbor analysis (CNA) [56]. Vacancy surface atoms were

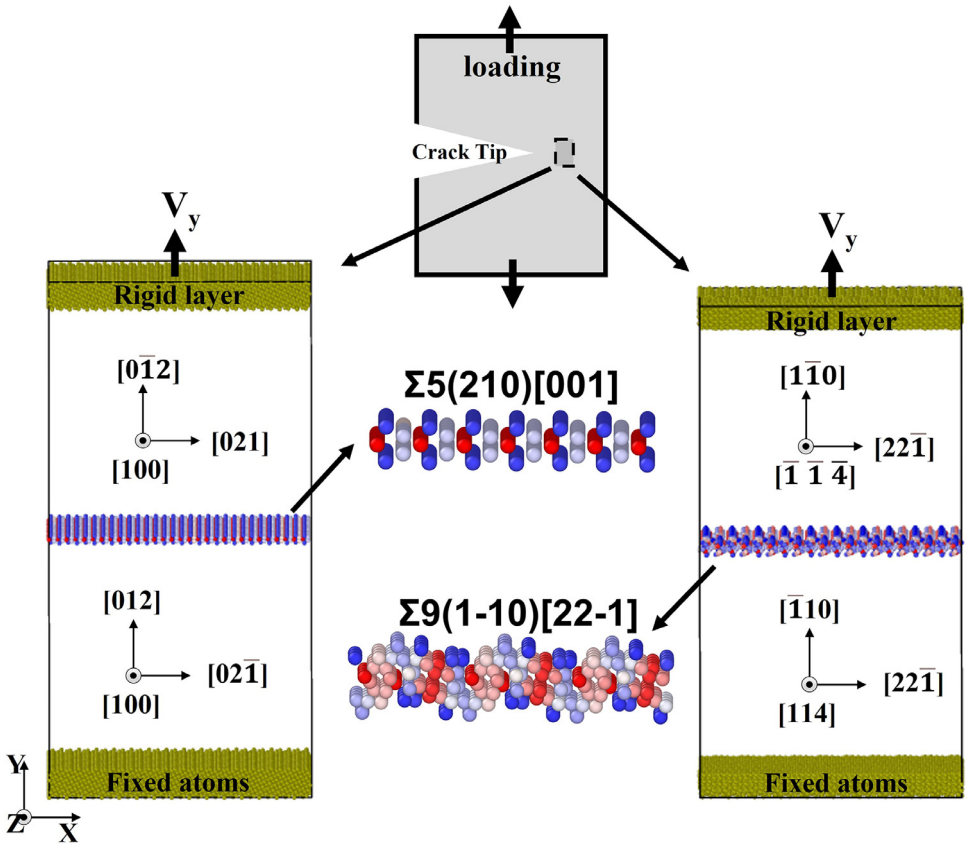

Fig. 1. Schematic of the atomistic models of nickel Σ5(210)[001] symmetric tilt and Σ9(1-10)[22-1] twist grain boundaries. Only atoms belonging to the GB are shown. The top and bottom are the rigid layers serving to apply deformation.

counted by calculating the coordination number of atoms in each snapshot after fast quenching and dislocations were identified with Ovito program [57].

3. Results and discussion

3.1. Hydrogen-induced transgranular to intergranular fracture transition

The dynamic GCMC/MD charging process with $\mu = -2.31$ *eV* is illustrated in Fig. 2c, d for the Σ5 and Σ9 GBs, respectively. The hydrogen concentration in the grains reached $c_0 = 0.001$ during the first 100,000 MC steps and stabilized gradually during the subsequent simulation steps. Meanwhile, hydrogen atoms keep pumping into the GB region due to the high excess volume and binding energy. After around 10,000,000 MC steps, hydrogen concentration at the Σ5 and Σ9 GBs also reached equilibrium (100% saturation) with $c = 0.240$ and $c = 0.215$, respectively. These two equilibrium GB configurations with saturated hydrogen in Fig. 2a are regarded as 100% (fully) charged cases at the chemical potential $\mu = -2.31$ *eV*. Apparently, a local hydrogen atmosphere has been formed around the Σ5 and Σ9 GB core, while the grain interior hydrogen concentration was slightly decreased to $c_0 = 0.0008$. The relationship between local equilibrium hydrogen concentration and applied chemical potential was further shown in Fig. 2b, agreeing with Eq. (1). These hydrogen distribution maps show good agreement with previous studies [31,58], where GBs are preferable accommodation sites for hydrogen.

After charging, uniaxial straining in the Y direction is applied on the bicrystal specimens at 300 K. This loading strategy provides a high stress triaxiality which mimics the stress state in the vicinity of a crack tip. During tension, plasticity occurs firstly with nucleation of 1/6<112> Shockley dislocations at the GBs (Fig. 3a_1, a_3, b_1, b_3). These dislocations enter the grains rapidly and interact with the top or bottom boundary, leaving stacking fault bands along the propagation pathway. As more dislocations nucleate and spread across the specimen, nanovoids start to nucleate, eventually leading to fracture. Compared to non-charged ones, hydrogen-charged samples are distinct both in mechanical response and in fracture mode. As shown in Fig. 3a and b, the first drop of the stress-strain curves corresponds to the first dislocation nucleation event as a sign of the onset of plasticity. Hydrogen facilitates the dislocation nucleation at Σ5 GB (first dislocation nucleates at strain $\varepsilon = 0.079$ and stress $\sigma_y = 11.06$ GPa in the hydrogen-free sample against $\varepsilon = 0.061$, $\sigma_y = 9.51$ GPa in the hydrogen charged specimen), while its influence on Σ9 GB seems negligible ($\varepsilon = 0.045$ and $\sigma_y = 8.48$ GPa without hydrogen versus $\varepsilon = 0.044$, $\sigma_y = 8.34$ GPa with hydrogen). In Fig.3 b_3, the dislocation nucleation at the lower half-grain will occur slightly later (0.001 strain) than in the upper grain. When the samples fracture by nanovoiding, the stress drops to zero. Hydrogen can significantly reduce the fracture stress and strain, and, more importantly, it switches the nanovoid nucleation site from the grain interior to GB (Fig. 3a_2, a_4, b_2, b_4). A distinctive companion of this process is the distortion of the crystal lattice in the vicinity of GB due to the accumulation of lattice defects. This distortion can be so significant that the translation symmetry breaks in some local regions leading to partial amorphization of the material as has been experimentally observed in hydrogen-charged steels [59,60] and nickel alloys [61,62]. In Fig. 3a_1, a_3, the local lattice distortion is noticed at the early stages of straining and is associated with the formation of Shockley dislocations and local HCP atomic packing. In Fig. 3a_4, b_4, the nanovoid at GB is formed

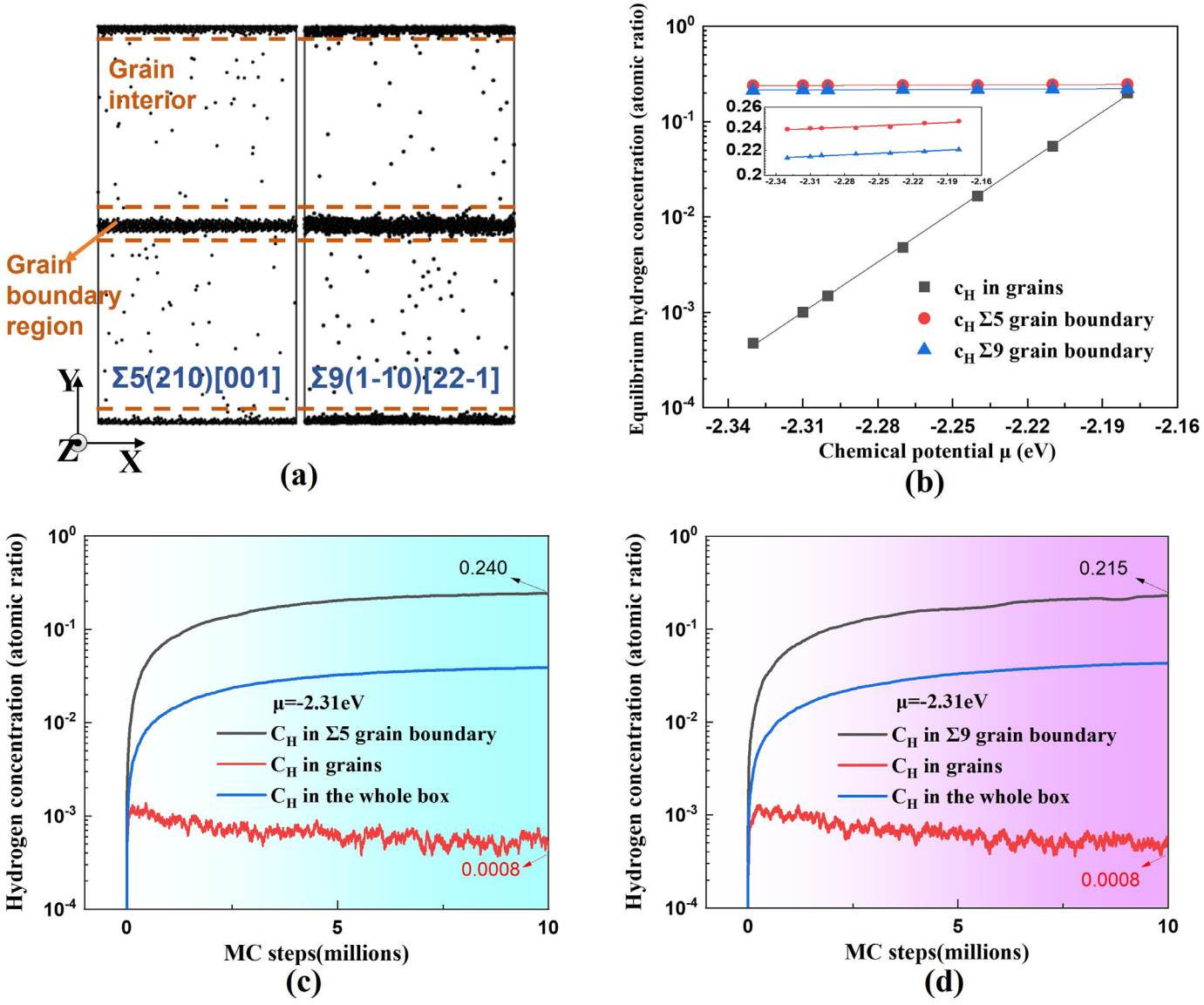

Fig. 2. (a) Equilibrium hydrogen distribution map around Σ5 and Σ9 GBs. Only hydrogen atoms are colored black. (b) The relationship between local equilibrium hydrogen concentration (H/Ni atomic ratio) and chemical potential. The relationship between equilibrium hydrogen concentration and chemical potential around Σ5 and Σ9 is highlighted in the inset. (c, d) Hydrogen concentration evolution around Σ5 and Σ9 GBs during GCMC/MD charging process.

by the expanding of those heavily distorted layers. The pivotal significance of the free volume associated with the excess vacancies and nanovoids in the local deformation and partial amorphization of the GB area will be further unfolded and clarified in Section 3.3. We repeat the simulation process 20 times with different random seeds for temperature. In the absence of hydrogen, transgranular fracture prevails over intergranular fracture: 19 out of 20 Σ5 samples, i.e., 95% of the samples, fail with nanovoid nucleation sites located inside the grains. The picture changes drastically in the presence of hydrogen: all 20 Σ5 samples fail with nanovoiding at GB. Thus, hydrogen enhances the intergranular fracture fraction from 5% to 100% for Σ5 GB at 300 K. This process is identified as the hydrogen-induced transgranular to intergranular fracture transition (see Supplementary movies 1 and 2). We should underline for clarity that the term "intergranular fracture" used in this study refers to the "intergranular nanovoiding" or "GB opening by nanovoiding" process, because the intergranular fracture occurs almost concurrently with the nanovoiding. This means the intergranular fracture here and below focuses only on the nanovoid nucleation behavior, which differs from the macroscopic intergranular fracture progressing through the void nucleation, coalescence, and crack propagation [3,63]. However, since the nanovoid nucleation is the prerequisite for void coalescence and crack propagation and since the nucleation site has been assigned to GB, the propensity for macroscopic intergranular fracture should also be enhanced.

3.2. Coupling effect of hydrogen and temperature

Both hydrogen and low temperature can cause embrittlement and intergranular fracture transition and their roles may be intertwined. We carried out simulations at various hydrogen concentrations and temperatures (77 K, 300 K, 600 K) to explore their coupling effect. Normalized hydrogen concentration at GB is defined as the relative ratio compared to the full saturation cases with Σ5 or Σ9 GBs. For instance, the 100% saturation at the Σ5 GB corresponds to a hydrogen concentration of $c = 0.240$. Hence, a normalized hydrogen concentration of 60% is equivalent to a concentration of $c = 0.144$. For each condition, 20 independent sim-

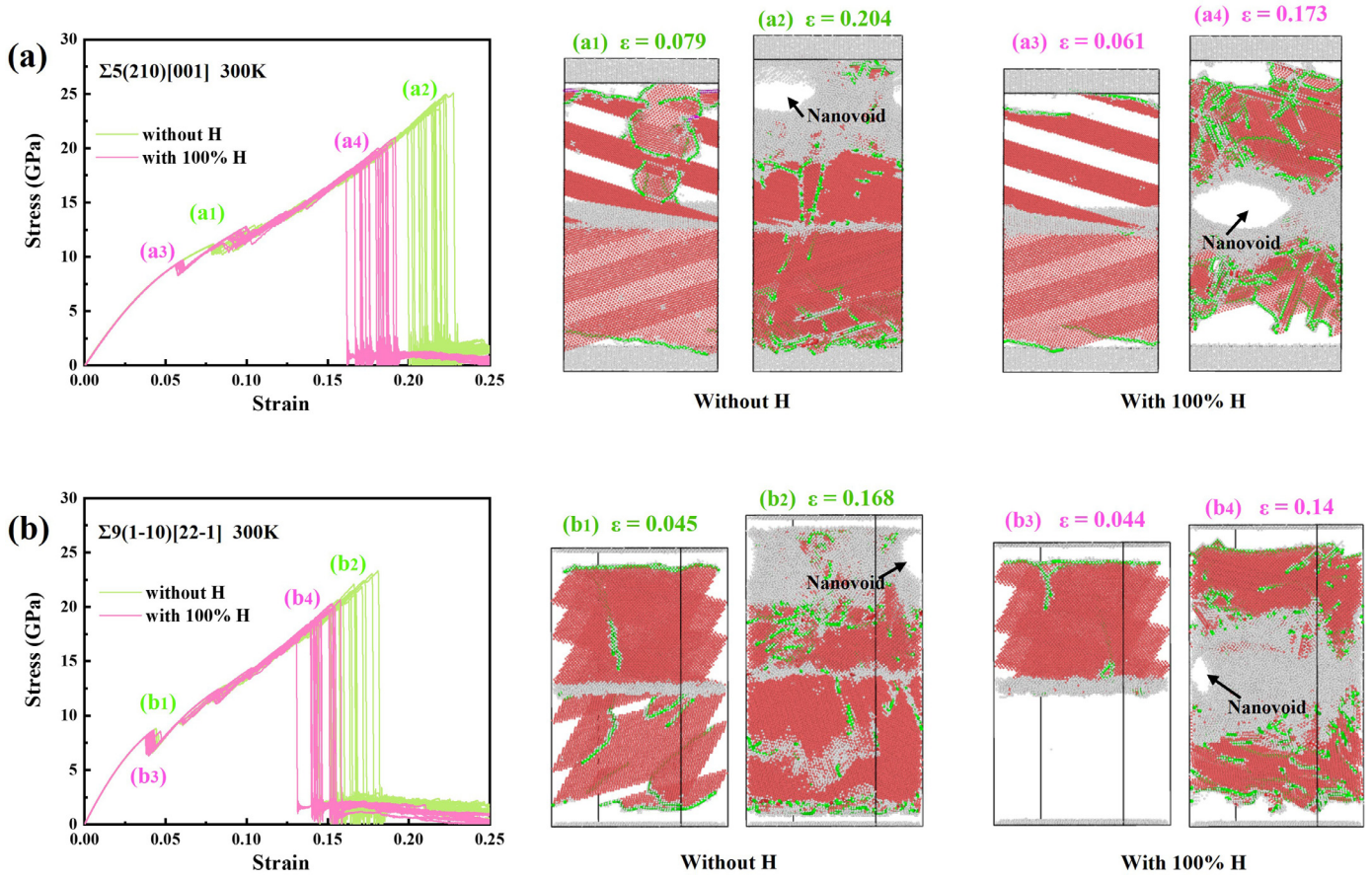

Fig. 3. Hydrogen-induced transgranular to intergranular facture transition: nanovoid nucleation site switching from grain interior to GB. (a, b) The stress-strain curves during uniaxial straining at 300 K for Σ5 and Σ9 GBs with and without hydrogen. Every line represents a MD simulation result with varying random seeds for temperature, which means all the atoms are given a different set of velocities according to the changed random seeds while the systems are kept at the same temperature of 300 K. (a_1, a_3, b_1, b_3) Snapshots show the events of first dislocation nucleation, corresponding to the first drop of stress in (a, b). (a_2, a_4, b_2, b_4) Snapshots show the events of nanovoid nucleation, corresponding to the maximum stress in (a, b). Atoms are colored by the common neighbor analysis parameters. FCC atoms are deleted, red HCP atoms indicate the glide paths of 1/6<112> Shockley dislocations (green pipelines), and grey atoms are in an amorphous structure.

ulations are performed to extract statistically reliable data. The coupling effect of hydrogen and temperature on dislocation nucleation varies depending on the GB type (Fig. 4a, d). Hydrogen could facilitate dislocation nucleation at the Σ5 GB with a more pronounced effect at 600 K, while Σ9 GB remains immune to hydrogen attack within the temperature range tested. In contrast, the coupling effect on nanovoid formation and final fracture manifests itself in a different manner (Fig. 4b, c, e, f). When sufficient hydrogen is charged, earlier fracture and increased proportions of intergranular fracture were observed. To avoid confusion with the customary notions where intergranular fracture usually addresses fractographic features indicative of the brittle nature of HE, the intergranular fracture in this study describes the GB opening process by nanovoiding accompanied by intense plasticity. Notably, the effect of hydrogen is always most pronounced at 77 K. This observation is consistent with the experimental results [29] that the hydrogen-promoted intergranular fracture was more frequently observed at low temperatures. However, the fact that hydrogen-enhanced dislocation nucleation and hydrogen-promoted earlier fracture have opposite temperature dependence suggests that hydrogen-dislocation interaction may not directly contribute to the final intergranular fracture. The change in the fracture mode should be attributed to other types of microstructural defects such as vacancies. This is elaborated in the subsequent sections.

3.3. Vacancy stockpiling at GB and its temperature dependence

A number of experimental observations [17,24,28] highlighted the importance of vacancy formation at GB. Here we explore the hydrogenated vacancies in the vicinity of GB and treat them as potential embryos for nanovoids. To quantify the evolution of vacancies at a deformed GB, the distorted atoms with coordination numbers less than 9 (featuring bond-breaking states) in the GB region are treated as vacancy surface atoms [33], and the fraction of these atoms is taken as the vacancy concentration. This definition differs from the conventional one for the vacancy-type of point defects, but it could well capture the amount of lattice distortions at GB, and give a comprehensive description of the enhanced excess free volume during GB amorphization [28,59,60]. Fig. 5b, g shows the distribution of vacancy surface atoms at GBs at a constant strain, as examples from the concentration plots in Fig. 5a, f. A dramatic increase in the number of vacancies is observed in all hydrogen-charged cases, with the maximum enhancement of over 10 times, as observed in the 100% saturated cases at 77 K for both Σ5 and Σ9 GBs. It should be noted that, to eliminate thermal noise, every snapshot is fast quenched to 10 K before calculating vacancy concentration. By repeating the quenching-and-calculating process for multiple times at different strains, we obtain the evolution of vacancy concentration as a function of strains in Fig. 5c–e, h–j. To avoid counting atoms on the nanovoid surface, we show only the

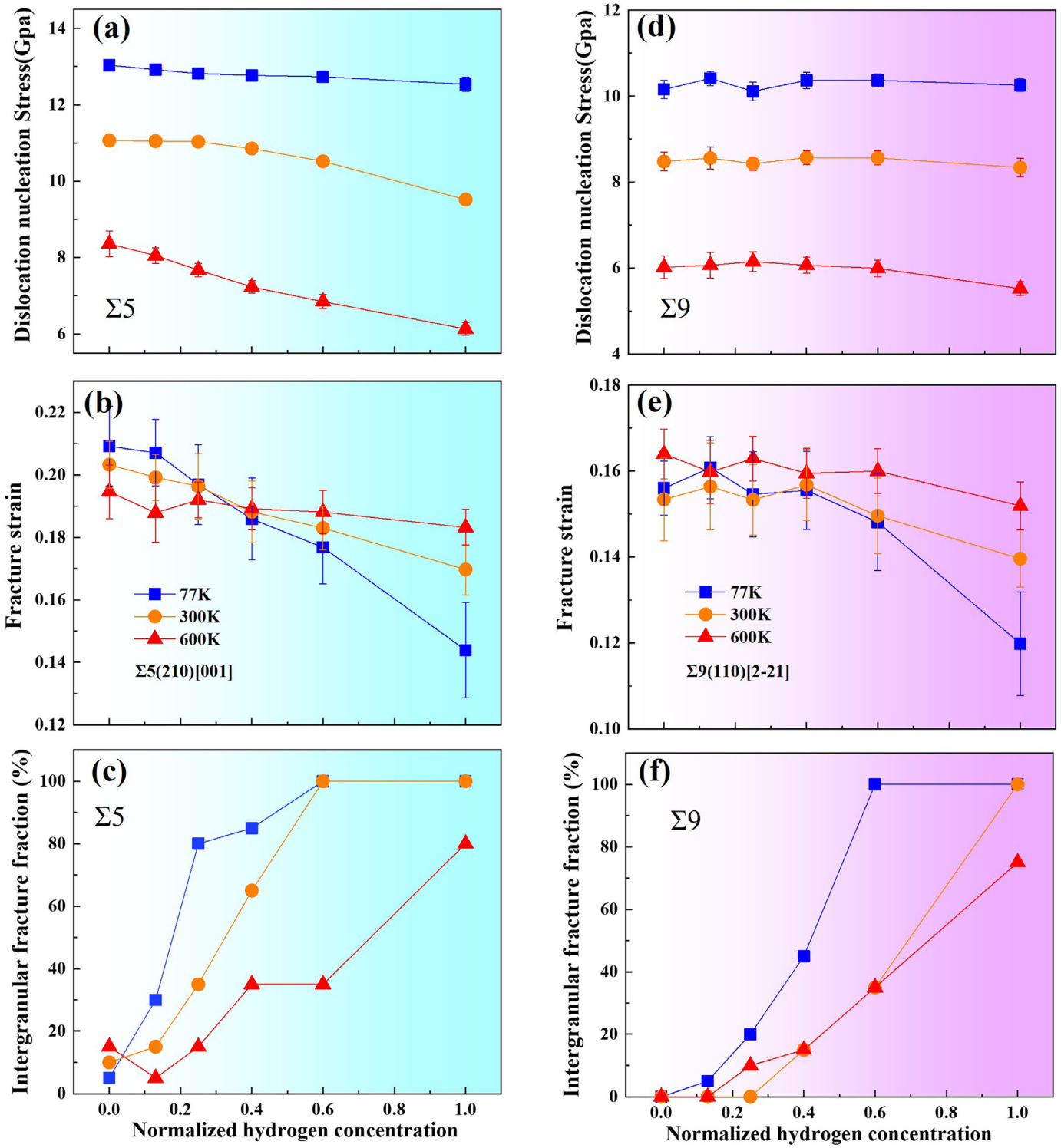

Fig. 4. The coupling effect of hydrogen and temperature on mechanical responses. (a, d) Dislocation nucleation stress is the critical stress for the first dislocation nucleation corresponding to the snapshots in Fig. 3(a_1, a_3, b_1, b_3). (b, e) Fracture strain is the strain for the onset of fracture, or on the other hand, failure corresponding to the snapshots in Fig. 3(a_2, a_4, b_2, b_4). (c, f) Fraction of intergranular fracture is a statistical quantity for samples exhibiting intergranular nanovoiding behavior. Hydrogen concentrations are normalized by the full saturation concentration at Σ5 and Σ9 GBs, respectively. The error bar on each data point in (a, b, d, e) indicates the standard deviation obtained from 20 independent simulations under the same conditions. All the samples are of the same size and a total amount of strain of 0.25 is applied to make sure that the nanovoid formation is observed in the course of deformation. The fraction of intergranular fracture is calculated as the proportion of samples with intergranular nanovoiding among the 20 independent simulations.

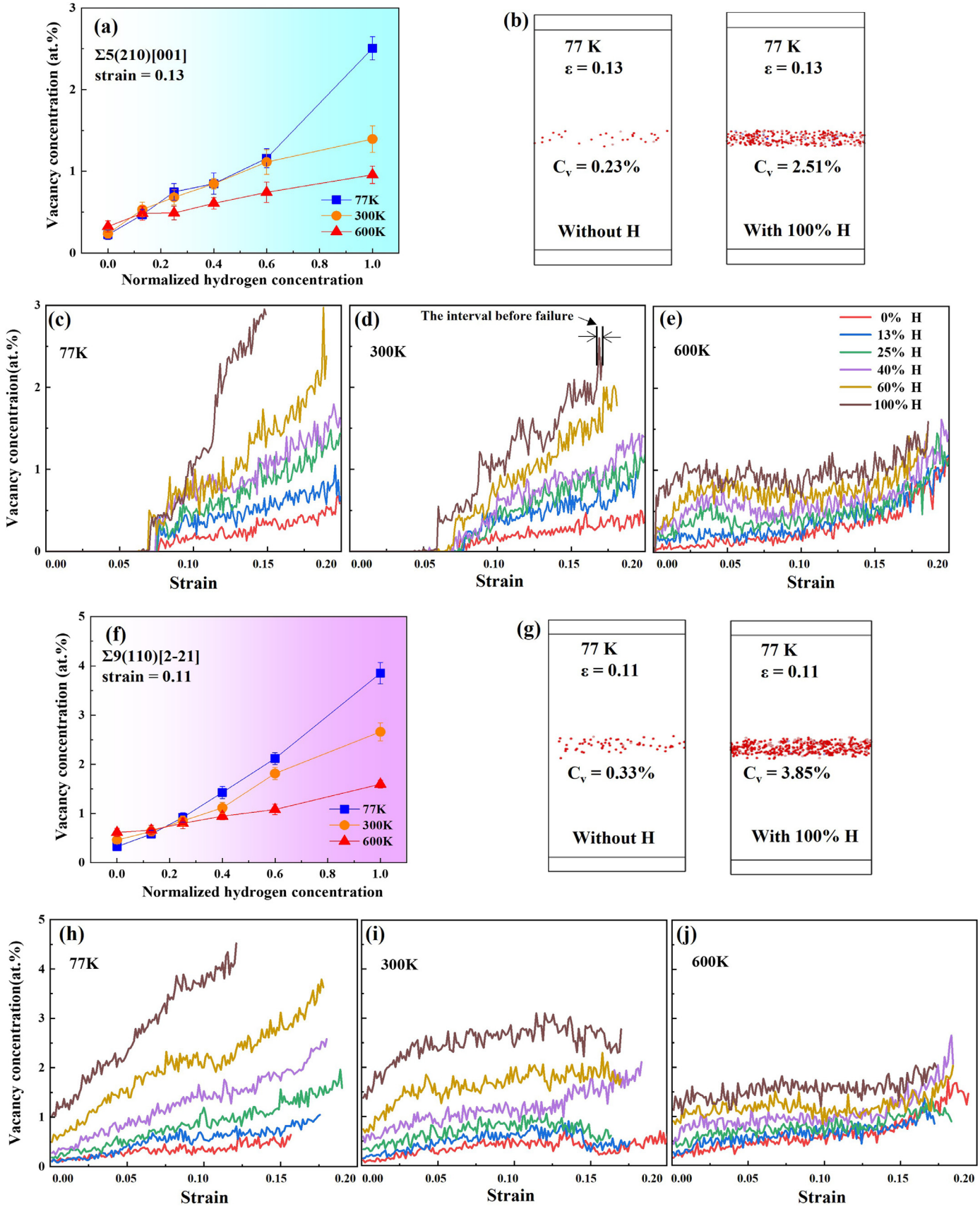

Fig. 5. Hydrogen-boosted vacancy stockpiling at GBs. (a,f) Vacancy concentration versus hydrogen concentration at different temperatures at the late plastic deformation stage. (b,g) Quenched snapshots illustrating the vacancy surface atoms for Σ5, 77 K, strain $\varepsilon = 0.13$ and Σ9, 77 K, strain $\varepsilon = 0.11$, respectively. Only highly distorted atoms with coordination numbers less than 9 in the GB region are colored. (c-e, h-j) Vacancy concentration evolves with strain under different conditions. Each data point in the figures is extracted from the fast quenched snapshots at the same strain.

strain range before failure. For the Σ5 GB at relatively low temperatures, 77 K and 300 K, vacancy is not observed at a small strain ($\varepsilon < 0.05$); the concentration starts to increase only after the onset of plasticity (Fig. 5c, d), and hydrogen acts as a powerful booster for the subsequent vacancy generation process. At 600 K, vacancies could be generated solely by hydrogen charging without external loading, and the vacancy concentration increases continuously at a very early stage (Fig. 5e). For the Σ9 GB, the insertion of hydrogen triggers vacancy generation at all three temperatures, while this only happens at 600 K for Σ5. This difference is caused by the less uniform structure of the Σ9 twist GB compared to the Σ5 symmetric tilt GB. Local plasticity could be activated during the elastic stage through self-amorphization before dislocation nucleation [64,65] at Σ9 GB. However, for the Σ5 boundary with a regular atomic structure, this deformation mechanism works only at high temperatures, where the conditions for sufficient thermal activation are fulfilled.

While hydrogen tends to persistently enhance the vacancy concentration, the temperature plays an intriguing dual role as either an enhancer or an inhibitor. In the absence of hydrogen, temperature increases lattice vibrations, and thus the probability of the thermally activated nucleation of lattice defects. The increased vacancy concentration can be expected at higher temperatures, where the highest vacancy concentration is observed at 600 K. When the specimen is pre-charged, the trapped hydrogen atoms reduce the vacancy formation energy by forming Va-H complexes, accelerating vacancy generation. Nevertheless, according to the previous thermodynamics work [66–68], those Va-H complexes become unstable at high temperatures and can dissociate into vacancy and interstitial hydrogen, which suppresses the role of hydrogen as a booster for vacancy generation. The enhanced diffusion at high temperature also accelerates the transport of hydrogen atoms from the GB region to the grain interior, driven by a decreased excess free volume ratio of GB [69,70]. This further restrains the influence of hydrogen at GB. All the above factors lead to the competition between thermal-activated vacancy generation and hydrogen detrapping mediated vacancy annihilation at elevated temperature, depending on the hydrogen concentration. As the concentration is low or zero, high temperature is favorable for strain-induced vacancy generation by thermal activation. When the concentration is high, however, low temperature becomes favorable, where detrapping of hydrogen is suppressed and the Va-H complex stays stable. These observations agree very well with the positron annihilation spectroscopy measurement [28] where grain refinement and cryogenic temperature amplify the hydrogen-enhanced vacancy effect and can be further rationalized with the equation for equilibrium vacancy concentration c_v:

$$c_v = g\exp\left(-\frac{E_v(c_H, \epsilon, T)}{k_b T}\right), \tag{2}$$

where g is the geometry factor depending on the arrangement of vacancies, E_v is a positive value of vacancy formation energy as a function of trapped hydrogen concentration c_H, local strain ϵ, and absolute temperature T. k_B is Boltzmann's constant. The magnitude of E_v reduces with increasing hydrogen concentration, favoring the formation of Va-H complex and an increasing c_v. Meanwhile, E_v increases with temperature, promoting the decomposition of Va-H complexes and decreasing c_v. In a heuristic way, one can assume that c_v is controlled primarily by temperature at low hydrogen concentration; at high concentration, the influence of hydrogen on vacancy formation prevails over the effect of temperature. This explains the trend observed earlier.

3.4. Critical vacancy concentration for intergranular fracture

To shed light on the relationship between vacancy stockpiling at GB and fracture mode, we extracted the vacancy concentration within the narrow strain interval before failure in Fig. 6a, c. The interval has a width of 0.01, as indicated in Fig. 5d, and the vacancy concentration is averaged within this strain interval prior to nanovoid nucleation. The vacancy concentrations show a similar dependence on hydrogen and temperature as in Fig. 5. Interestingly is that a fully intergranular fracture (with 100% frequency of observations) is observed when a sufficient number of vacancies is accumulated at GB. All these vacancy concentrations are measured and plotted against the intergranular fracture fraction in Fig. 6b, d. Surprisingly, both Σ5 and Σ9 GBs reveal an S-shape correlation between the intergranular fracture fraction and the vacancy concentration. At the low vacancy concentration (below 1.0% for Σ5 and 1.5% for Σ9), which usually means a low hydrogen concentration, the transgranular fracture mode prevails. Vacancies mainly nucleate and coagulate to form nanovoids in the grain interior; while the number of vacancies at GB is small. As the vacancy concentration increases (to 1.0% $\sim$ 1.7% for the Σ5 and 1.5% $\sim$ 2.8% for Σ9), the intergranular fracture fraction increases rapidly. At this stage, the concentrations of both hydrogen and vacancies reach high values, and hydrogen further promotes vacancy agglomeration at GB. Nanovoid nucleation at GB eventually wins the competition over that in grain interior. As the vacancy concentration exceeds a certain critical value (of 1.7% for Σ5 and 2.8% for Σ9, respectively), the fully intergranular fracture is observed. In this regime, all the samples fail intergranularly. We should note that all vacancy concentrations used in the above considerations are still defined in the local region close to the GB ($\pm$ 1 nm). The existence of this critical value reveals the pivotal role played by vacancies in the hydrogen-induced transgranular to intergranular facture transition. Understanding of this fact can be further utilized to predict the nanovoid nucleation site. That is, if we can estimate the vacancy concentration based on its relationship with hydrogen concentration and temperature, c.f., Fig. 6a, c, or through direct measurements, then it is possible to compare the estimated or measured value of the vacancy concentration with the simulated critical value to unveil the proportion of the intergranular fracture in all samples. Take the Σ9 GB for example, the critical vacancy concentration is about 2.8 at.%. The normalized hydrogen concentration for achieving this vacancy concentration is about 0.6 for T =77K and 1 for T =300K, respectively. Considering that the real hydrogen concentration is 0.215 corresponding to a normalized hydrogen concentration of 1 for Σ9, we obtain the critical hydrogen concentration for the intergranular fracture in the Σ9 GB, which is 0.129 for T =77K and 0.215 for T =300K, respectively. Those critical hydrogen concentrations can be utilized as the threshold for intergranular fracture transition. Another interesting observation is that at high temperature, e.g. T =600K, the critical hydrogen concentration does not exist; in other words, it is impossible to have fully intergranular fracture. These findings also explain the recent observations made in low-temperature HE experiments [28,29] where the hydrogen-dislocation interaction was highly suppressed whereas the intergranular fracture was still observed. The rationale standing behind this observation is that it is the enhanced vacancy generation due to hydrogen that made a major contribution to the increased propensity towards intergranular failure.

3.5. Role of dislocations in vacancy stockpiling

Further analysis is carried out to elucidate the relationship between dislocation activity in grains and vacancy evolution at GB. Fig. 7a, b show the atomic structures and the vacancy distribution in the Σ5 GB case at 300 K. Before dislocation nucleation, there

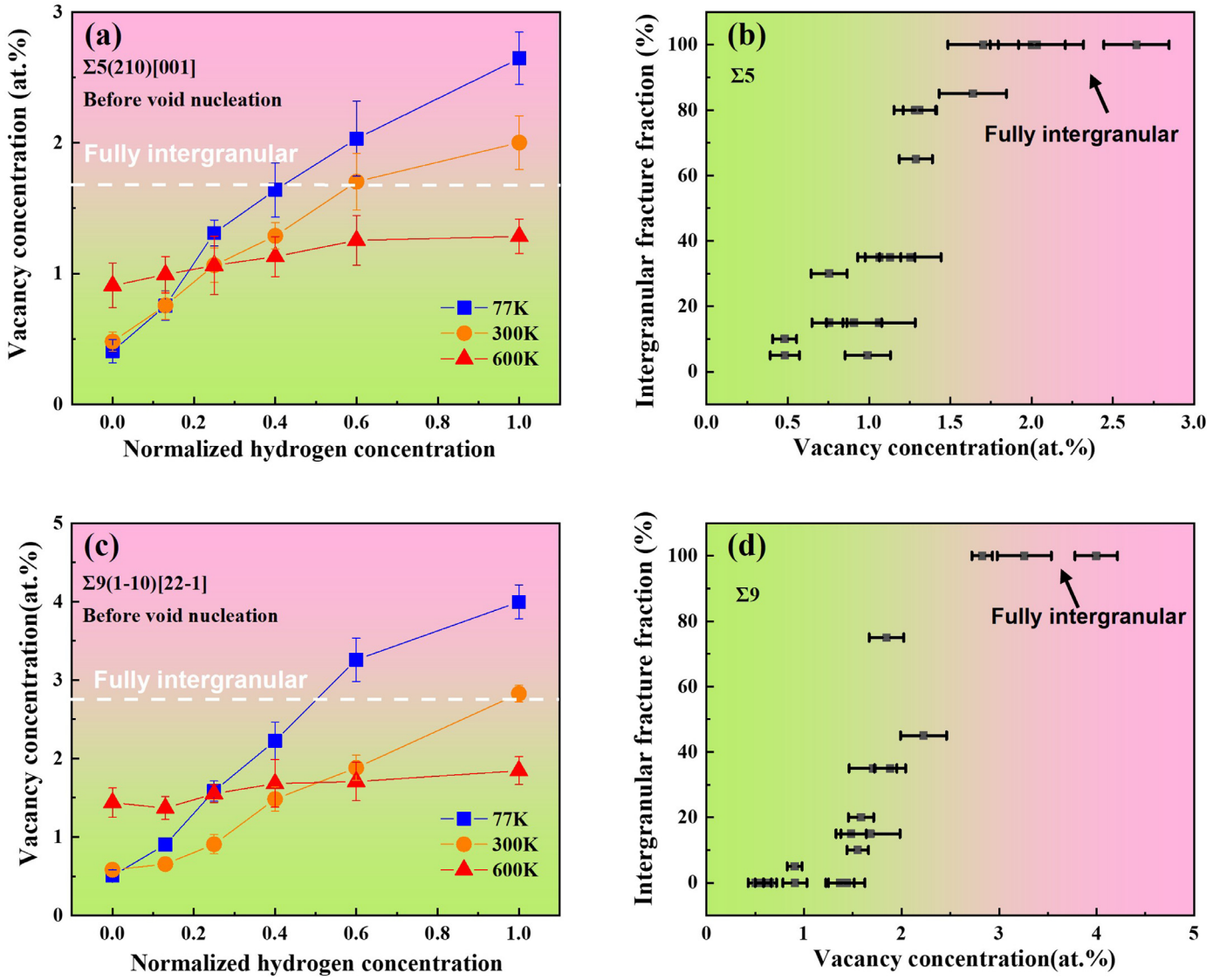

Fig. 6. GB vacancy stockpiling is responsible for intergranular fracture. (a, c) GB vacancy concentration before nanovoid nucleation versus varying hydrogen concentrations and temperatures. Each data point is collected at a point right before fracture. (b, d) Relationship between intergranular fracture fraction and vacancy concentration at GB. Intergranular fracture fraction becomes 100% as critical vacancy concentration (1.7% for Σ5 and 2.8% for Σ9) is reached, i.e. all the samples are expected to fail by intergranular fracture. Error bars correspond to the standard deviation of 20 individual simulations under the same conditions.

are few vacancies at the GB, with or without hydrogen. Once plasticity emerges in the grains, the vacancy concentration increases rapidly, with line-shaped vacancy clusters occurring at sites where dislocations nucleated. In the presence of hydrogen, the vacancy clusters become more distinguished, indicating enhanced vacancy multiplication. The enhancement is often thought to be mediated by hydrogen enhanced dislocation activity, in line with the HESIV theory. This assumption is also examined. We take the fraction of HCP atoms along the dislocation path as an indicator of dislocation glide volume, i.e., the amount of dislocation activity. Every sudden increase or drop of this indicator signifies the interaction between dislocations and GB. Fig. 7c–h show the evolution of vacancy concentration and dislocation glide volume. Surprisingly, the enhancement due to hydrogen on the amount of dislocation activity in all the cases is limited, while the enhancement due to hydrogen on vacancy generation is far more pronounced. It is particularly the case for the Σ9 GB and for the Σ5 GB at 600K. As mentioned earlier, the generation of vacancies is thermally activated in these cases, which can be triggered by hydrogen charging [71]. Hydrogen increases the vacancy concentration by multiple times, even before plasticity occurs. It appears that hydrogen-enhanced vacancy generation in these cases is not related to dislocation nucleation or in other words, plasticity in the grains. It is more likely that hydrogen directly participates in the thermodynamics of vacancy formation and interacts with existing vacancies, whether there is plasticity or not. In other words, plasticity does not seem to be a premise for this to happen. Deviation appears in the case of Σ5 GB at 77K and 300K. There is no vacancy formation before the onset of plasticity with or without hydrogen. Then the vacancy concentration suddenly increases accompanied by a rise in dislocation glide volume in Fig. 7c, d, approximately at a strain of 0.07. This applies also to hydrogen-free cases. The development of vacancies aligns very well with plasticity in the grains. This alignment shows the important role of GB-dislocation interaction in producing vacancies but is still insufficient to explain the large enhancement in vacancy generation, considering that the enhancement in dislocation activity is still limited. Those observations show good agreement with recent experimental measurements [72]. All these cases convey the same important message that hydrogen enhanced vacancy generation in Σ5 and Σ9 GBs primarily has to do with the direct interaction be-

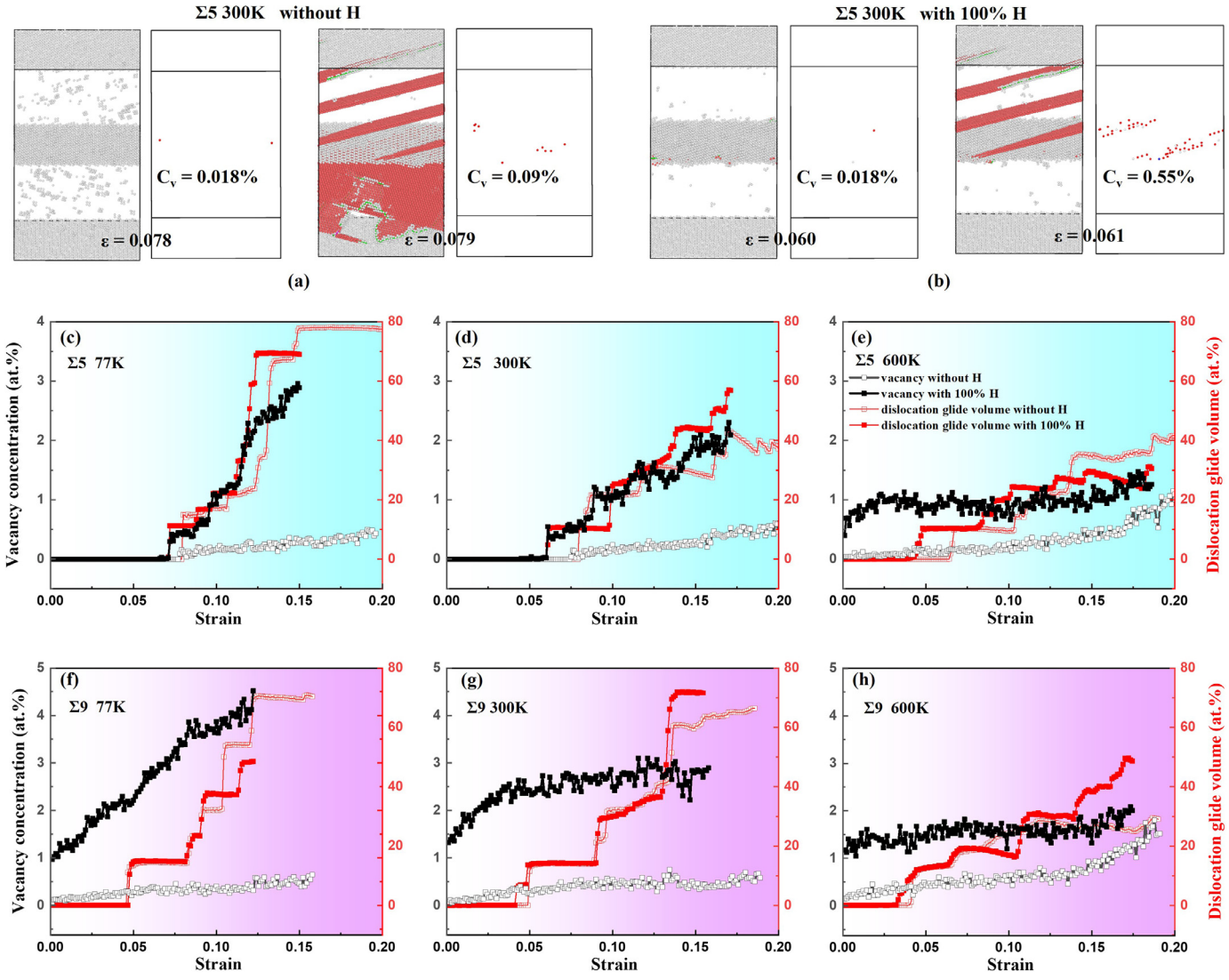

Fig. 7. Effects of hydrogen on vacancy generation and dislocation activity. (a,b) Snapshots of atomic structures and vacancy distributions for the Σ5 GB at 300 K. (c-h) Vacancy concentration and dislocation glide volume evolutions in the absence and presence of hydrogen for different conditions. Dislocation glide volumes are obtained by calculating the fraction of atoms through which dislocations have traveled.

tween hydrogen and existing vacancies, while the interaction with dislocations does not seem to be a prerequisite.

4. Conclusion

Through atomistic simulations on the interaction between hydrogen and two types of representative GBs, we were able to probe the nanoscale mechanism of hydrogen-induced transgranular to intergranular fracture transition. Hydrogen-boosted vacancy stockpiling at GB is revealed to be responsible for the increased propensity towards intergranular failure. This process can be termed hydrogen-enhanced vacancy stockpiling-induced nanovoiding mechanism, which is in harmony with the recent experimental studies [73–75]. During straining, vacancies are generated in the vicinity of GBs as a result of dislocation-GB interaction giving rise to local GB amorphization. Hydrogen works as a promoting agent for vacancy generation and can enhance vacancy concentration at GB by up to 10 times. The subsequent vacancy agglomeration causes earlier nanovoid formation at GB, which otherwise should nucleate in a much later stage inside the grains. This proposed mechanism covers the interactions among hydrogen, dislocations, vacancies, and GB, which is essential for interpreting experimental observations. It should be noted that this mechanism is not in conflict with the existing theories, rather, it should be regarded as a synergistic action of HELP, HESIV, and HEDE mechanisms, although there may be certain discrepancies when compared to a single mechanism. For example, the HELP mechanism emphasizes the role of hydrogen-enhanced plasticity in establishing the condition for final failure. In this study, we did observe intense dislocation activities beneath the fracture surface. However, the hydrogen effect on dislocation gliding is limited. The main effect of hydrogen-dislocation interaction is exerted at the GB, which increases the vacancy concentration and furnishes the condition for final decohesion. Compared to hydrogen which persistently boosts the vacancy generation, temperature plays a dual role depending on the charged hydrogen level. When hydrogen concentration is low, temperature facilitates vacancy generation by thermal activation. While at a high hydrogen level, temperature inhabits vacancy formation by destabilizing the Va-H complex. This temperature dependence revealed in our simulations is in good agreement with the recent PAS experiments [28]. Furthermore, a GB-specific quantitative relation between the probability of intergranular fracture and vacancy concentration under different conditions was further drawn. It highlights the existence of critical va-

cancy concentration acting as a threshold for the complete intergranular fracture and enables the quantitative prediction of HE in polycrystalline materials. A case in point is, given the microstructure (GB type and fraction), temperature and loading, it is possible to utilize the critical vacancy concentration to calculate the threshold hydrogen concentration for intergranular fracture. In summary, by quantitative analysis of the time-resolved microstructure evolution, we pinpoint the key role of vacancy stockpiling in HE and provide a vacancy-based criterion for hydrogen-induced intergranular fracture.

Data availability

The data that support the findings of this study are available from the corresponding authors upon request.

Declaration of Competing Interest

The authors declare that they have no known competing financial interests or personal relationships that could have appeared to influence the work reported in this paper.

CRediT authorship contribution statement

Yu Ding: Visualization, Formal analysis, Writing – original draft. **Haiyang Yu:** Supervision, Project administration, Writing – original draft. **Meichao Lin:** Writing – original draft. **Kai Zhao:** Writing – original draft. **Senbo Xiao:** Writing – original draft. **Alexey Vinogradov:** Writing – original draft. **Lijie Qiao:** Writing – original draft. **Michael Ortiz:** Writing – original draft. **Jianying He:** Supervision, Project administration, Writing – original draft. **Zhiliang Zhang:** Supervision, Project administration, Writing – original draft.

Acknowledgments

Y.D. acknowledge the financial support provided by the Research Council of Norway under the M-HEAT project (Grant No. 294689) and the HyLINE project (Grant No. 294739). All simulations are carried out on the Fram (Grant No. NN9110K, NN9391K) high-performance computer clusters at NTNU, Trondheim.

Supplementary materials

Supplementary material associated with this article can be found, in the online version, at doi:10.1016/j.actamat.2022.118279.

References

[1] W.H. Johnson, On some remarkable changes produced in iron and steel by the action of hydrogen and acids, Proc. R. Soc. Lond. 23 (156-163) (1875) 168–179.
[2] R.P. Gangloff, B.P. Somerday, Gaseous Hydrogen Embrittlement of Materials in Energy Technologies: Mechanisms, Modelling and Future Developments, Elsevier, 2012.
[3] S. Lynch, Hydrogen embrittlement phenomena and mechanisms, Corros. Rev. 30 (3-4) (2012) 105–123.
[4] R. Kirchheim, Reducing grain boundary, dislocation line and vacancy formation energies by solute segregation. I. Theoretical background, Acta Mater. 55 (15) (2007) 5129–5138.
[5] I.M. Robertson, P. Sofronis, A. Nagao, M.L. Martin, S. Wang, D.W. Gross, K.E. Nygren, Hydrogen embrittlement understood, Metall. Mater. Trans. B-Process Metall. Mater. Process. Sci. 46 (3) (2015) 1085–1103.
[6] M.B. Djukic, G.M. Bakic, V.S. Zeravcic, A. Sedmak, B. Rajicic, The synergistic action and interplay of hydrogen embrittlement mechanisms in steels and iron: localized plasticity and decohesion, Eng. Fract. Mech. 216 (2019).
[7] R. Oriani, A mechanistic theory of hydrogen embrittlement of steels, Ber. Bunsenges. Phys. Chem. 76 (8) (1972) 848–857.
[8] S. Serebrinsky, E.A. Carter, M. Ortiz, A quantum-mechanically informed continuum model of hydrogen embrittlement, J. Mech. Phys. Solids 52 (10) (2004) 2403–2430.
[9] J. Song, W.A. Curtin, Atomic mechanism and prediction of hydrogen embrittlement in iron, Nat. Mater. 12 (2) (2013) 145–151.
[10] A. Tehranchi, X. Zhou, W.A. Curtin, A decohesion pathway for hydrogen embrittlement in nickel: mechanism and quantitative prediction, Acta Mater. 185 (2020) 98–109.
[11] M. Lin, H. Yu, Y. Ding, G. Wang, V. Olden, A. Alvaro, J. He, Z. Zhang, A predictive model unifying hydrogen enhanced plasticity and decohesion, Scr. Mater. 215 (2022) 114707.
[12] D. Wan, Y. Deng, J.I.H. Meling, A. Alvaro, A. Barnoush, Hydrogen-enhanced fatigue crack growth in a single-edge notched tensile specimen under *in-situ* hydrogen charging inside an environmental scanning electron microscope, Acta Mater. 170 (2019) 87–99.
[13] Z. Zhang, Z. Yang, S. Lu, A. Harte, R. Morana, M. Preuss, Strain localisation and failure at twin-boundary complexions in nickel-based superalloys, Nat. Commun. 11 (1) (2020) 1–11.
[14] H.K. Birnbaum, P. Sofronis, Hydrogen-enhanced localized plasticity - a mechanism for hydrogen-related fracture, Mat. Sci. Eng. A Struct. 176 (1-2) (1994) 191–202.
[15] M.L. Martin, M. Dadfarnia, A. Nagao, S. Wang, P. Sofronis, Enumeration of the hydrogen-enhanced localized plasticity mechanism for hydrogen embrittlement in structural materials, Acta Mater. 165 (2019) 734–750.
[16] J. Song, W.A. Curtin, Mechanisms of hydrogen-enhanced localized plasticity: an atomistic study using alpha-Fe as a model system, Acta Mater. 68 (2014) 61–69.
[17] D. Xie, S. Li, M. Li, Z. Wang, P. Gumbsch, J. Sun, E. Ma, J. Li, Z. Shan, Hydrogenated vacancies lock dislocations in aluminium, Nat. Commun. 7 (1) (2016) 13341.
[18] X. Lu, D. Wang, D. Wan, Z.B. Zhang, N. Kheradmand, A. Barnoush, Effect of electrochemical charging on the hydrogen embrittlement susceptibility of alloy 718, Acta Mater. 179 (2019) 36–48.
[19] Y. Ding, H. Yu, K. Zhao, M. Lin, S. Xiao, M. Ortiz, J. He, Z. Zhang, Hydrogen-induced transgranular to intergranular fracture transition in bi-crystalline nickel, Scr. Mater. 204 (2021) 114122.
[20] S. Wang, M.L. Martin, I.M. Robertson, P. Sofronis, Effect of hydrogen environment on the separation of Fe grain boundaries, Acta Mater. 107 (2016) 279–288.
[21] A. Tehranchi, W. Curtin, Atomistic study of hydrogen embrittlement of grain boundaries in nickel: I. Fracture, J. Mech. Phys. Solids 101 (2017) 150–165.
[22] M.L. Martin, B.P. Somerday, R.O. Ritchie, P. Sofronis, I.M. Robertson, Hydrogen-induced intergranular failure in nickel revisited, Acta Mater. 60 (6-7) (2012) 2739–2745.
[23] Y. Fukai, Formation of superabundant vacancies in M–H alloys and some of its consequences: a review, J. Alloys Compd. 356 (2003) 263–269.
[24] M. Nagumo, Hydrogen related failure of steels - a new aspect, Mater. Sci. Technol. Lond. 20 (8) (2004) 940–950.
[25] M. Nagumo, K. Takai, The predominant role of strain-induced vacancies in hydrogen embrittlement of steels: overview, Acta Mater. 165 (2019) 722–733.
[26] S.Z. Li, Y.G. Li, Y.C. Lo, T. Neeraj, R. Srinivasan, X.D. Ding, J. Sun, L. Qi, P. Gumbsch, J. Li, The interaction of dislocations and hydrogen-vacancy complexes and its importance for deformation-induced proto nano-voids formation in alpha-Fe, Int. J. Plast. 74 (2015) 175–191.
[27] Y.X. Zhu, Z.H. Li, M.S. Huang, H.D. Fan, Study on interactions of an edge dislocation with vacancy-H complex by atomistic modelling, Int. J. Plast. 92 (2017) 31–44.
[28] S.K. Lawrence, Y. Yagodzinskyy, H. Hanninen, E. Korhonen, F. Tuomisto, Z.D. Harris, B.P. Somerday, Effects of grain size and deformation temperature on hydrogen-enhanced vacancy formation in Ni alloys, Acta Mater. 128 (2017) 218–226.
[29] Z.D. Harris, S.K. Lawrence, D.L. Medlin, G. Guetard, J.T. Burns, B.P. Somerday, Elucidating the contribution of mobile hydrogen-deformation interactions to hydrogen-induced intergranular cracking in polycrystalline nickel, Acta Mater. 158 (2018) 180–192.
[30] Y. Ogawa, K. Noguchi, O. Takakuwa, Criteria for hydrogen-assisted crack initiation in Ni-based superalloy 718, Acta Mater. (2022) 117789.
[31] Y.S. Chen, H. Lu, J. Liang, A. Rosenthal, H. Liu, G. Sneddon, I. McCarroll, Z. Zhao, W. Li, A. Guo, Observation of hydrogen trapping at dislocations, grain boundaries, and precipitates, Science 367 (6474) (2020) 171–175.
[32] H. Zhao, P. Chakraborty, D. Ponge, T. Hickel, B. Sun, C.H. Wu, B. Gault, D. Raabe, Hydrogen trapping and embrittlement in high-strength Al alloys, Nature 602 (7897) (2022) 437–441.
[33] L. Wan, W.T. Geng, A. Ishii, J.P. Du, Q.S. Mei, N. Ishikawa, H. Kimizuka, S. Ogata, Hydrogen embrittlement controlled by reaction of dislocation with grain boundary in alpha-iron, Int. J. Plast. 112 (2019) 206–219.
[34] A. Tehranchi, W.A. Curtin, The role of atomistic simulations in probing hydrogen effects on plasticity and embrittlement in metals, Eng. Fract. Mech. 216 (2019) 106502.
[35] S. Yin, G.M. Cheng, T.H. Chang, G. Richter, Y. Zhu, H.J. Gao, Hydrogen embrittlement in metallic nanowires, Nat. Commun. 10 (2019).
[36] X.S. Kong, S. Wang, X. Wu, Y.W. You, C. Liu, Q. Fang, J.L. Chen, G.N. Luo, First-principles calculations of hydrogen solution and diffusion in tungsten: temperature and defect-trapping effects, Acta Mater. 84 (2015) 426–435.
[37] W. Geng, L. Wan, J.P. Du, A. Ishii, N. Ishikawa, H. Kimizuka, S. Ogata, Hydrogen bubble nucleation in α-iron, Scr. Mater. 134 (2017) 105–109.
[38] J. Hou, X.S. Kong, X.B. Wu, J. Song, C.S. Liu, Predictive model of hydrogen trapping and bubbling in nanovoids in bcc metals, Nat. Mater. 18 (8) (2019) 833–839.

[39] S. Taketomi, R. Matsumoto, N. Miyazaki, Atomistic study of hydrogen distribution and diffusion around a {1 1 2}< 1 1 1>edge dislocation in alpha iron, Acta Mater. 56 (15) (2008) 3761–3769.
[40] J. Von Pezold, L. Lymperakis, J. Neugebeauer, Hydrogen-enhanced local plasticity at dilute bulk H concentrations: the role of H–H interactions and the formation of local hydrides, Acta Mater. 59 (8) (2011) 2969–2980.
[41] P. Yu, Y.G. Cui, G.Z. Zhu, Y. Shen, M. Wen, The key role played by dislocation core radius and energy in hydrogen interaction with dislocations, Acta Mater. 185 (2020) 518–527.
[42] B. Kuhr, D. Farkas, I.M. Robertson, Atomistic studies of hydrogen effects on grain boundary structure and deformation response in FCC Ni, Comput. Mater. Sci. 122 (2016) 92–101.
[43] K.N. Solanki, M.A. Tschopp, M.A. Bhatia, N.R. Rhodes, Atomistic investigation of the role of grain boundary structure on hydrogen segregation and embrittlement in alpha-Fe, Metall. Mater. Trans. A 44a (3) (2013) 1365–1375.
[44] J. Li, C. Lu, L. Pei, C. Zhang, R. Wang, Atomistic investigation of hydrogen induced decohesion of Ni grain boundaries, Mech. Mater. 150 (2020) 103586.
[45] R. Matsumoto, S. Taketomi, S. Matsumoto, N. Miyazaki, Atomistic simulations of hydrogen embrittlement, Int. J. Hydrog. Energy 34 (23) (2009) 9576–9584.
[46] J. Song, W. Curtin, Mechanisms of hydrogen-enhanced localized plasticity: an atomistic study using α-Fe as a model system, Acta Mater. 68 (2014) 61–69.
[47] A. Tehranchi, W. Curtin, Atomistic study of hydrogen embrittlement of grain boundaries in nickel: II. Decohesion, modelling and simulation in, Mater. Sci. Eng. 25 (7) (2017) 075013.
[48] J.E. Angelo, N.R. Moody, M.I. Baskes, Trapping of hydrogen to lattice-defects in nickel, Model. Simul. Mater. Sci. 3 (3) (1995) 289–307.
[49] W. Shinoda, M. Shiga, M. Mikami, Rapid estimation of elastic constants by molecular dynamics simulation under constant stress, Phys. Rev. B 69 (13) (2004) 134103.
[50] M.Q. Chandler, M.F. Horstemeyer, M.I. Baskes, P.M. Gullett, G.J. Wagner, B. Jelinek, Hydrogen effects on nanovoid nucleation in face-centered cubic single-crystals, Acta Mater. 56 (1) (2008) 95–104.
[51] M. Koyama, S.M. Taheri-Mousavi, H. Yan, J. Kim, B.C. Cameron, S.S. Moeini-Ardakani, J. Li, C.C. Tasan, Origin of micrometer-scale dislocation motion during hydrogen desorption, Sci. Adv. 6 (23) (2020) eaaz1187.
[52] S. Plimpton, Fast parallel algorithms for short-range molecular-dynamics, J. Comput. Phys. 117 (1) (1995) 1–19.
[53] D.J. Adams, Grand canonical ensemble monte-carlo for a lennard-jones fluid, Mol. Phys. 29 (1) (1975) 307–311.
[54] A.P. Thompson, S.J. Plimpton, W. Mattson, General formulation of pressure and stress tensor for arbitrary many-body interaction potentials under periodic boundary conditions, J. Chem. Phys. 131 (15) (2009) 154107.
[55] C.L. Kelchner, S.J. Plimpton, J.C. Hamilton, Dislocation nucleation and defect structure during surface indentation, Phys. Rev. B 58 (17) (1998) 11085–11088.
[56] J. Schiotz, F.D. Di Tolla, K.W. Jacobsen, Softening of nanocrystalline metals at very small grain sizes, Nature 391 (6667) (1998) 561–563.
[57] A. Stukowski, Visualization and analysis of atomistic simulation data with OVITO–the open visualization tool, Modell. Simul. Mater. Sci. Eng. 18 (1) (2009) 015012.
[58] D. Di Stefano, M. Mrovec, C. Elsasser, First-principles investigation of hydrogen trapping and diffusion at grain boundaries in nickel, Acta Mater. 98 (2015) 306–312.
[59] M. Nagumo, T. Ishikawa, T. Endoh, Y. Inoue, Amorphization associated with crack propagation in hydrogen-charged steel, Scr. Mater. 49 (9) (2003) 837–842.
[60] A. Harada, K. Kusunoki, K. Moritani, K. Matsumoto, M. Hatano, Y. Horibe, Amorphization under fracture surface in hydrogen-charged and low-temperature tensile-tested austenitic stainless steel, Philos. Mag. Lett. 101 (1) (2021) 40–50.
[61] K. Young, T. Ouchi, H. Shen, L. Bendersky, Hydrogen induced amorphization of LaMgNi4 phase in metal hydride alloys, Int. J. Hydrog. Energy 40 (29) (2015) 8941–8947.
[62] Y. Li, H. Ren, Y. Zhang, Z. Liu, H. Zhang, Hydrogen induced amorphization behaviors of multiphase La0. 8Mg0. 2Ni3. 5 alloy, Int. J. Hydrog. Energy 40 (22) (2015) 7093–7102.
[63] T. Neeraj, R. Srinivasan, J. Li, Hydrogen embrittlement of ferritic steels: Observations on deformation microstructure, nanoscale dimples and failure by nanovoiding, Acta Mater. 60 (13-14) (2012) 5160–5171.
[64] R. Benedictus, A. Böttger, E. Mittemeijer, Thermodynamic model for solid-state amorphization in binary systems at interfaces and grain boundaries, Phys. Rev. B 54 (13) (1996) 9109.
[65] M.Y. Gutkin, I. Ovid'Ko, Disclinations, amorphization and microcrack generation at grain boundary junctions in polycrystalline solids, Philos. Mag. A 70 (4) (1994) 561–575.
[66] J.M. Polfus, O.M. Løvvik, R. Bredesen, T. Peters, Hydrogen induced vacancy clustering and void formation mechanisms at grain boundaries in palladium, Acta Mater. 195 (2020) 708–719.
[67] D. Tanguy, Y. Wang, D. Connetable, Stability of vacancy-hydrogen clusters in nickel from first-principles calculations, Acta Mater. 78 (2014) 135–143.
[68] N. Fernandez, Y. Ferro, D. Kato, Hydrogen diffusion and vacancies formation in tungsten: density functional theory calculations and statistical models, Acta Mater. 94 (2015) 307–318.
[69] A. Oudriss, J. Creus, J. Bouhattate, E. Conforto, C. Berziou, C. Savall, X. Feaugas, Grain size and grain-boundary effects on diffusion and trapping of hydrogen in pure nickel, Acta Mater. 60 (19) (2012) 6814–6828.
[70] H. Sun, C.V. Singh, Temperature dependence of grain boundary excess free volume, Scr. Mater. 178 (2020) 71–76.
[71] L. Chiari, K. Kojima, Y. Endo, H. Teshigahara, M. Butterling, M.O. Liedke, E. Hirschmann, A.G. Attallah, A. Wagner, M. Fujinami, Formation and time dynamics of hydrogen-induced vacancies in nickel, Acta Mater. (2021) 117264.
[72] Y. Sugiyama, K. Takai, Quantities and distribution of strain-induced vacancies and dislocations enhanced by hydrogen in iron, Acta Mater. 208 (2021) 116663.
[73] S. Jothi, S. Merzlikin, T. Croft, J. Andersson, S. Brown, An investigation of micro-mechanisms in hydrogen induced cracking in nickel-based superalloy 718, J. Alloys Compd. 664 (2016) 664–681.
[74] D.M. Symons, A.W. Thompson, The effect of hydrogen on the fracture of alloy X-750, Metall. Mater. Trans. A 27 (1) (1996) 101–110.
[75] T. Homma, T. Chiba, K. Takai, E. Akiyama, W. Oshikawa, M. Nagumo, Cracking process in delayed fracture of high-strength steel after long atmospheric exposure, ISIJ Int. (2022) ISIJINT-2021-238.